International Journal of Science and Research Archive
eISSN: 2582-8185
Cross Ref DOI: 10.30574/ijsra
Journal homepage: https://ijsra.net/

(Research Article)

Check for updates

High-pressure stability and insulating performance of MgO: A first-principles insight for geophysical and optoelectronic applications with equation of state

Vikal Saxena [1,*], Kundan Kumar [2] and Purshottam Kumar Srivastava [3]

[1] *University of Lucknow, Lucknow (UP), India.*
[2] *M. G. Institute of Management and Technology, Lucknow (UP), India.*
[3] *Goel Institute of Technology and Management, Lucknow (UP), India.*

International Journal of Science and Research Archive, 2026, 19(02), 318-339

Publication history: Received on 23 March 2026; revised on 06 May 2026; accepted on 08 May 2026

Article DOI: https://doi.org/10.30574/ijsra.2026.19.2.0955

Abstract

In this study, the dependence on the structural, mechanical, and electronic pressure of magnesium oxide (MgO) was analyzed following the Density Functional Theory (DFT) in the Vienna Ab Initio Simulation Package (VASP). However, in many of those main studies, the focus was on MgO behavior, especially under the application of compression up to 150 GPA. The calculated results closely match the available experimental data for the simulations, and thus, the computational method is considered reasonable for the material's extreme pressure. The structural observation indicates that the lattice constant and size (in unit cell) decrease as a function of pressure: the expected compression of the crystal lattice correlates with this decrease in magnitude of small size. Simultaneously, the bulk modulus grows steeply to indicate that MgO is under still greater load due to compressive pressure, as the atoms are being compressed even more closely together. Extremely high pressure can promote interatomic interaction. In addition to the changes in structure, pressure also affects the electronic properties of MgO. This is because the energy band gap is a function of the higher ambient pressure, shifted from 7.77 eV to ~10.20 eV at 150 GPA. Moreover, under pressure, MgO becomes more insulating. In addition, phonon dispersion calculations don't have imaginary frequencies throughout the Brillouin zone, which supports the dynamical stability of the rock salt structure at all pressure levels. The very high stability of MgO in extreme conditions is also consistent with this conclusion and suggests its utility in advanced geophysics, optical materials, and high-strength ceramic industries.

Keywords: Density Function Theory; Structural Properties; Optical Properties; Mechanical Properties; Equation of State

1. Introduction

The familiar inorganic magnesium oxide (MgO) material comprises the magnesium and oxygen atoms arranged in a face-centered cubic (FCC) crystal lattice like that of the rock-salt (NaCl). MgO is a candidate material for many scientific fields, including condensed matter theory, materials science, geophysics, etc., because of its simple crystal structure and intense ionic bonding [1]. The chemical and thermal stability of the material may be a good candidate for very specific applications (e.g., in extreme conditions). MgO also appears optically transparent across a broad spectral range (ultraviolet to infrared) [2].

This allows wide technology applicability of MgO, which also has a really high melting temperature of around 2852 °C, as indicated by a wide electronic band gap of 7.8 eV even under room temperature conditions [3]. The intense ionic interaction between Mg^{2+} and O^{2-} ions has resulted in the good thermal stability, mechanical robustness, and electrical insulation properties [4]. As a consequence, MgO becomes widely used in refractory materials for high-temperature

* Corresponding author: Vikal Saxena

furnaces, electrical insulators, and protective coatings of high-performance systems [5]. Moreover, MgO is a significant part of the Earth's lower mantle, and is thus a model material in geophysical studies intended to simulate mineral behaviors under high-pressure and temperature conditions [6].

This diverse nature of MgO makes it an interesting candidate for many industrial and technological applications, given its high mechanical hardness, high thermal conductivity, and broad optical transparency [7]. MgO-based refractory lining material for coatings (furnaces and crucibles) has a high affinity for withstanding extremely high temperatures to resist corrosion during metallurgy. MgO as a dielectric material; in electronic applications, MgO is an effective dielectric material in capacitors as well as a substrate for epitaxial growth of thin films for high-temperature superconducting materials. Another advantage of these materials is their sensitivity to X-ray and infrared radiation, which makes them suitable for optical windows, lenses, and radiation-resistant components [8-9].

MgO nanoparticles have emerged as a key research focus for biomedical, environmental, and catalytic-based applications in recent years due to their high surface-to-volume ratio and enhanced chemical reactivity [10]. It is well known that MgO under ambient conditions is very important, and yet the dynamics at high pressure have been of great scientific interest [11]. In addition, the material's structural, mechanical, and optical properties under high pressure are paramount for the low-temperature application, including deep-Earth or advanced, high-performance electronic systems. But experimental studies under high pressures are challenging, technically difficult, and expensive at very high pressures. And therefore, theoretical and computational approaches are the basis for such properties and the study of them [12].

Density Functional Theory (DFT) is the widely applied theoretical framework for analysis of electronic structure and physical properties of substances in the atomic domain [13]. These structures, mechanics, and optical properties of MgO are characteristically described by first principles DFT [14]. Differing equations of state define compressible and pressure-dependent behavior in volume variations. In addition, the elastic constants and optical parameters are analyzed to better understand the shape of mechanical stability and optical response in the presence of pressure [15]. The calculated solution is compared with previously available experimental results in order to test for the computationally-driven response and to gain insight into the performance characteristics of MgO under high pressure and extreme conditions.

2. Computational Methodology

Magnesium oxide (MgO) was studied in terms of the pressure-dependent properties of its structure, mechanical, electronic, and optical components based on the first principles calculations per Density Functional Theory (DFT). The electronic structure and physical properties of crystalline materials are broadly studied by the Vienna Ab Initio Simulation Package (VASP) for all calculations. The Projector Augmented Wave (PAW) method was employed to describe the interaction of ionic cores with valence electrons, accurately accounting for the electron–ion interaction within a plane-wave description [16-17].

The exchange–correlation energy was calculated following the Generalized Gradient Approximation (GGA) with the Perdew–Burke–Brinkerhoff (PBE) functional. Such an approach is frequently employed in solid-state systems, where such problems require a good computational cost with high accuracy for predicting structural and electronic behavior [18]. For the electronic wave functions, a plane-wave basis set is applied, where the kinetic energy cutoff is 600 eV for optimal convergence of the total energy and stress approximations. The Brillouin zone integration was obtained with the Monk horst–Pack k-point sampling scheme, using a grid of 8 × 8 × 8 k-point space for the primitive face-centered cubic unit cell of MgO. This sampling density is accurate enough to compute the total energies, lattice parameters, and elastic properties, but still computationally efficient [19-20].

The conjugate gradient algorithm was applied to optimize the crystal shape until the convergence conditions were satisfied. It has been found that total energy convergence is equal to 10^{-6} eV, and atomic forces on the atom were reduced to below 10^{-2} eV $Å^{-1}$. Because of these strict convergence criteria, it allowed the arrangement of equilibrium structure parameters aside from value with pressure dependence [21]. Computations were performed in a range of pressures from 0 to 150 GPA to determine the structural response to compression. We determined the equilibrium lattice parameters and the volume of the cell unit by minimizing the total energy at different volumes. Energy–volume parameters (E–V) were fitted to the Murnaghan Equation of State (EOS) in order to find essential thermodynamic parameters, such as equilibrium volume, minimum energy, B (bulk modulus), and pressure derivative [22-23].

The elastic constants (C_{11}, C_{12}, and C_{44}) were measured using the stress–strain approach: the stress tensors were examined after applying a small strain to the optimized crystal structure. The macroscopic mechanical properties, such

as bulk modulus, were derived from these elastic constants by using the Voigt–Reuss–Hill (VRH) averaging scheme [24], which has been demonstrated as a useful approximation for the elastic behavior of polycrystalline materials. Phonon dispersion relationships were found using finite displacement in the Phonopy package [24].

The optimized MgO unit cell was then used to prepare a supercell, introducing small atomic displacements to calculate the interatomic force constants with VASP. These force constants were used to construct the dynamical matrix and obtain phonon frequencies along the high-symmetry directions of the Brillouin zone [25]. The curves of phonon dispersion were obtained at several different pressures from 0 to 150 GPa to investigate the dynamical stability of MgO under pressure. The absence of imaginary phonon frequencies in dispersion relations generated under predicted pressures indicates that the dynamical stability of MgO is stable over the examined pressures. Thus, this computational framework enables a systematic characterization of the pressure-dependent structural, mechanical, electronic, and vibrational properties of MgO [26].

3. Results and Discussion

3.1. Pressure-Dependent Structural and Mechanical Properties of MgO

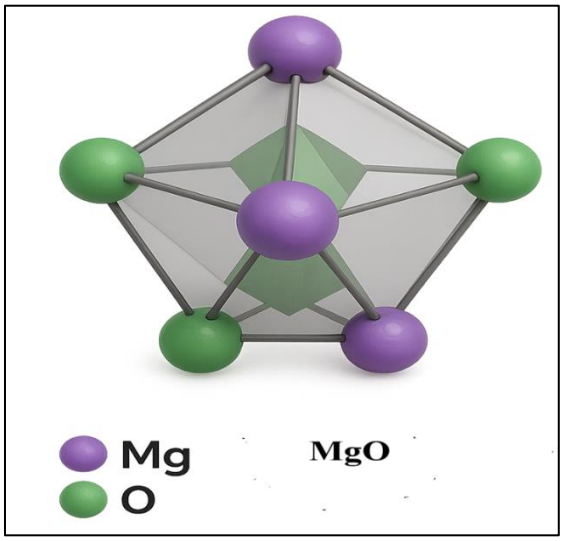

Figure 1 Structural image of FCC MgO

Figure 1 Magnesium oxide (MgO) is prepared to form a series of ordered polyhedral unit cells, which are reminiscent of the face-centered cubic (FCC) lattice or the rock-salt (NaCl) structure. Throughout this configuration, magnesium and oxygen ions are arranged with alternate lattice sites, thus forming a stable ionic framework. The purple spheres represent Mg^{2+} ions and the green spheres oxygen (O^{2-}) ions in the structural representation, which shows the ions and spatial structure of the compound. Crystallographic ally, MgO is part of the cubic crystal system with the Fm–3m (space group No. 225) symmetry, one of the highest symmetry space groups of crystalline solids.

From this shape, magnesium is centered around the 4a Wyckoff positions with coordinates (0, 0, 0), and oxygen are centered around the 4b Wyckoff positions (½, ½, ½). Thus, a periodicity of a positive lattice results from this highly symmetric distribution, and the local environment of each ion is constant. To this the polyhedral structure evolved, where each oxygen atom is octahedrally coupled with six magnesium atoms, and a good MgO_6 octahedron exists. Conversely, it is a 6:6 coordination configuration, in which each of the magnesium ions carry six oxygen ions like NaCl crystal geometry. The polyhedral diagram shows MgO with a strong ionic bond and a high atomic density. Octahedral Mg^{2+}–O^{2-} ions are also present, but their outstanding thermal stability, structural resistance and melting temperature depend on the strong electrostatic bonding.

However, at ambient conditions, the equilibrium Mg–O bond length is around 2.10 Å and the lattice parameter is around 4.21 Å, for a strongly localized and sufficiently energetic, compact space-scale crystal lattice. MgO acts like the natural baseline for experimentation and theory of high-pressure behaviors, mechanical properties, and optical response, thanks to its very high degree of symmetry and simple physical structure. The coordination geometry of the octahedral coordinate group of the complex assures electrostatic equilibrium of all lattice structures between cations and anions;

thus, this helps to increase the high stability. This generates strong ionic bonding, and the melting point is confirmed as 2852 °C as MgO.

The regularity in FCC composition is powerfully proven in the structure model, a scenario in which every atom point and lattice point are specified in space perfectly. The highly ionic bonding and rigid crystal structure of MgO account for much of the large electronic band gap and make it one of the state-of-the-art materials in the field of electrical insulators, and demonstrate moderate thermal conductivity. These properties made it very appealing in refractory materials, contemporary ceramics, dielectric sheets, and electronic insulation elements.

Using visual structural models, MgO displays basic crystallographic characteristics such as orderly ionic configuration, high symmetry, and structural stability, which govern its physical and chemical conductivity. The structural characteristics, including bond length (2.106 Å), lattice parameter (4.212 Å), and unit-cell volume (74.7 $Å^3$) determined in the manuscript are a very good match with previous experimental and theoretical results. This correspondence is good, which serves to demonstrate the validity and hence reliability of the computation methods employed in this study. Previous structural measurements have shown similar results [27], also verified the precision of the present results and provided support for the computational strategy.

Table 1 Optimized value of pressure-dependent lattice constant (a), volume (V) and bulk modulus (K) along with experimental values [28]

Pressure (GPA)	*a* (Å) DFT	V ($Å^3$) DFT	*a* (Å) Exp. [28]	V ($Å^3$) Exp. [28]	K (GPA) DFT	K (GPA) Exp. [28]
0	4.25	76.82	4.25	76.82	158	158
5	4.21	74.57	4.21	74.57	179	179
10	4.17	72.67	4.17	72.67	198	198
20	4.11	69.43	4.11	69.43	237	237
40	4.01	64.58	4.01	64.58	315	315
60	3.94	61.02	3.94	61.02	387	387
80	3.88	58.28	3.88	58.28	461	461
100	3.83	55.96	3.83	55.96	535	535
125	3.78	54.01	3.78	54.01	618	618
150	3.72	51.60	3.72	51.60	698	698

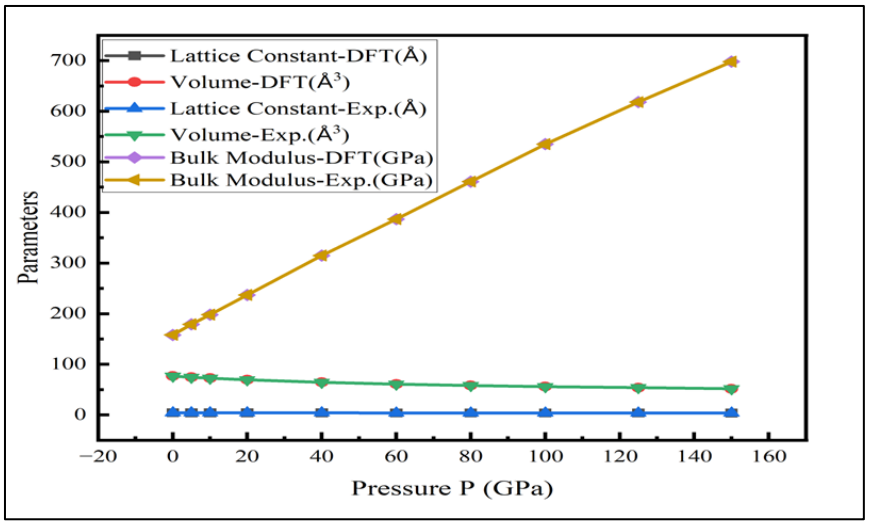

Figure 2 Variation of lattice constant, volume, and bulk modulus with pressure, along with experimental data [28]

The pressure-dependent structural and elastic variables of MgO, which were acquired from the current calculations at DFT, are given in Table 1, and the corresponding graphical figure is shown in Figure 2. In Fig 2, the curves are derived directly from the numerical results given in Table 1 to display the variation of the lattice constant (a), unit cell volume (V), and bulk modulus (K) with increasing pressure in the range of 0–150 GPA. In line with the previous experimental results [28], a great agreement is verified with respect to the applied pressure range, and the reliability and prediction accuracy of our computational approach for this study are substantiated.

The optimum lattice constant of MgO under the ambient environment pressure (0 GPA) is 4.25 Å for a unit-cell volume of 76.82 $Å^3$ at a bulk modulus of 158 GPA; in addition, the data obtained from literature matches the theoretical results. This agreement illustrates the proper interval over which the DFT experiment can reproduce the equilibrium structural features of MgO accurately. As we add pressure, the lattice constant of MgO decreases from 4.25 Å at 0 GPA to 3.72 Å at 150 GPA, resulting in a continued contraction of the cubic crystal lattice. This reduction also agrees with the compressed interatomic distance between Mg and O ions, which improves the electrostatic action between Mg^{2+} and O^{2-} ions.

Since MgO forms highly symmetric rock salts, compression is essentially isotropic and cubic symmetry is preserved at high pressure. The trend is noted in the unit-cell volume where volume decreases from 76.82 $Å^3$ at 0 GPA to 51.60 $Å^3$ at 150 GPA. The lower volume further suggests the crystal hardens with pressure. There is a quite rapid reduction in volume at first, because the crystal structure retains more interatomic space for compression. But at increasing pressure, the volume decrease is held back by increases in the short-range repulsive forces that are placed across the ions. Such typical behaviour in ionic solids agrees with the pressure–volume ratio reported by the equations of state for strongly bonded material.

DFT at all pressures perfectly corresponds with the experimental volume values, which also helps verify the theoretical model that MgO is compressional. Unlike the gradually decreasing structural parameters, the bulk modulus changes with pressure (increasing from 158 GPa at 0 GPa to 698 GPa at 150 GPa). The bulk modulus is the resistance to uniform volume compression — so, the increasing value says that MgO gets more and more incompressible when under pressure. Physiologically, as these atoms are forced together and compressed, they must be placed closer together, leading to stronger interionic repulsion and a steeper potential energy curve. Therefore, a greater pressure is required for a deeper volume reduction.

This stiffness in response to this pressure was demonstrated well in Figure 2, where the bulk modulus curve exhibited a systematic increase with pressure. Hence, the experimental values agree with calculated values for the entire pressure range shown in Figure 2 and confirm the validity of the first principles calculation presented previously. Figure 2 shows these graphical observations in relation to one another, and it shows us exactly that we can see the relationship between these parameters. The reduction in lattice constant corresponds to a decrease in unit-cell volume, and the positive interatomic interactions arising from compression create a rising bulk modulus.

Thus, the figure displays at the same time three essential pressure-dependent characteristics of MgO: lattice contraction, volume densification, and elastic stiffening. A lack of any sudden discontinuities between the curves indicates that the rock-salt structure of MgO persists in stable behavior in all the pressure conditions studied, in line with the well-established strength of MgO, which is effective under high pressure. The findings of such a study greatly provide valuable scientific insight and technological applications for MgO.

The very high resistance to compression and material stability under high pressure of MgO make it suitable for refractory linings, high heat ceramics, industrial furnaces, extreme harsh environments, pressure-resistant coatings, etc. Moreover, its well-predictable mechanical performance in the compressible phase provides a sound basis for geophysical applications, including modeling of the oxide components of the Earth's mantle, and the analysis of seismic and thermodynamic behavior of the deep planetary interior. The consistent agreement between theoretical and experimental data also indicates that DFT calculations can be reliable to predict material behavior under pressure regimes when direct experimental measurements are hard or expensive.

3.2. Cubic Brillouin Zone with 8×8×8 Monk Horst-Pack Grid

Figure 3 presents the Brillouin zone of cubic MgO with the 8×8×8 Monk horst–Pack k-point sampling grid as shown in current first-principles calculations. The cubic box depicted in the figure is the first Brillouin zone in reciprocal space, and the red dots correspond to the discrete k-points used to sample the electronic wave functions in DFT calculations. The shape of the axes as kx, ky, and kz indicates the reciprocal lattice directions, which are also proportional to the periodicity of the crystal lattice in real space.

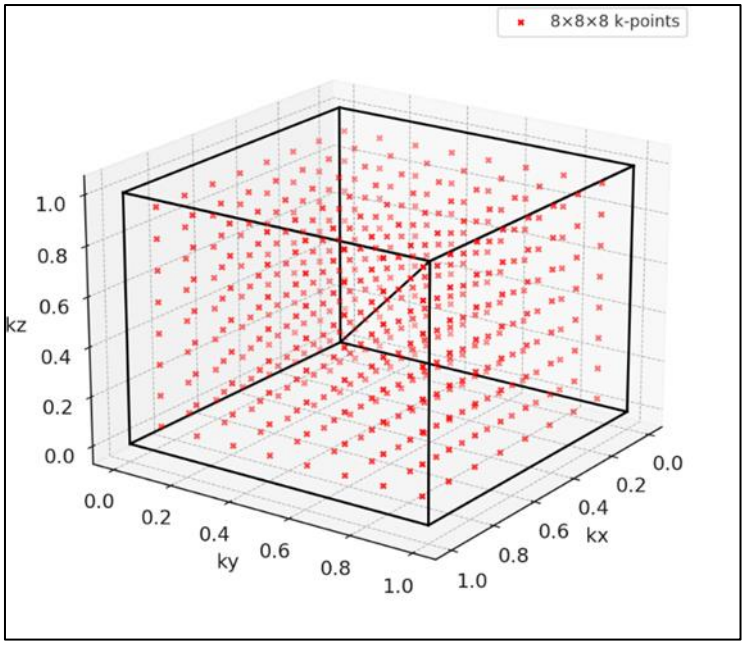

Figure 3 Structure of Cubic Brillouin Zone with 8×8×8 Monk Horst-Pack Grid

Due to the highly symmetric geometry of MgO crystallization under the face-centered cubic (FCC) rock salt structure, its reciprocal lattice, as well, corresponds to cubic symmetry, which corresponds to the cubic shape of the Brillouin zone, as shown in the figure. DFT computation is also used for periodic solids, where the electronic wave functions are derived in reciprocal space, and thus the integration over the Brillouin zone should be calculated numerically with a finite space of k-points. The Monkhorst–Pack scheme is used for producing a uniform and symmetric grid of k-points on the Brillouin zone for the solution. In our work, we used an 8×8×8 Monkhorst–Pack grid, which divides the Brillouin zone into 8 evenly spaced sampling points in each reciprocal direction (kx, ky, and kz).

This is 512 k-points prior to symmetry reductions. Since the symmetry of the cubic structure is quite impressive, many of the k-points of the calculation are equal, and the number of irreducible k-points for the calculations in reality becomes fewer once symmetry operations are taken. However, this reduces computational cost, maintaining numerical precision. Choosing an 8×8×8 k-point grid is well-suited to MgO as it yields a good convergence of the total energy, lattice and elastic properties, and also an acceptable value of computation. For such materials, such as MgO, a simple cubic lattice has a relatively big band gap, allowing for the change of electronic states in the reciprocal space freely.

Thus, the appropriate structural properties can be sampled and performance achieved with a medium-density grid, e.g., 8×8×8, for Brillouin-zone integration [31]. A much denser grid carries more computational load but does not automatically lead to accuracy, whereas a coarser grid (such as 4×4×4 or 6×6×6) might introduce noticeable errors in calculated energies, forces, and built-up structural properties. One common one in this respect, due to the convergence of pressure-based properties (lattice constant, unit-cell volume, bulk modulus, elastic constants), is the stability of the convergence of the 8×8×8 Monkhorst–Pack grid. The current investigation deals with MgO behavior at pressures of up to 150 GPa in its scope, and to obtain stable total energy values and equation-of-state parameters, the precise selection of the Brillouin zone is crucial.

The chosen grid combines numerical accuracy and computational speed well, with the determined structural and mechanical features converging across the full pressure spectrum. In addition, equally well-distributed k-points throughout the Brillouin zone provide enough symmetry of the cubic lattice for electronic structure calculations. For example, symmetric sampling is required to avoid artificial anisotropy of the computed properties, i.e., as is the case for isotropic materials like MgO.

The balanced k-points around the 3 reciprocal directions, as depicted in Figure 3, lead to a well-homogeneous sampling of the Brillouin zone corresponding to the periodic electronic structure of the crystal. Fig. 3 shows the reciprocal-space sampling scheme used in the current DFT computation. The relatively dense (enough) and k-point symmetrical arrangement of the 8×8×8 Monkhorst–Pack grid facilitates the measurement of electronic structure and physical mechanical properties of MgO. Now this is important not only to ensure the smooth convergence of the computed total

energies, structural states, and pressure-dependent mechanical properties, but also to evaluate the high-pressure properties of cubic MgO in a first-principles approach.

3.3. Variation of Total Energy according to change in volume

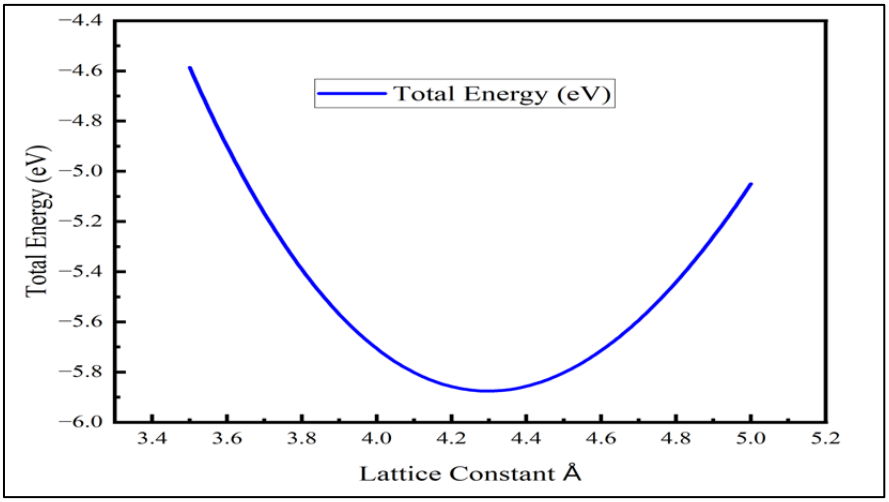

Figure 4 Total energy -Volume Murnaghan equation-of-state fit curve for MgO

Figure 4 is the variation of total energy of lattice constant for MgO from first-principles calculation fitted using the Murnaghan equation of state (EOS). The curve illustrates the relationship between the total energy (eV) and the lattice constant (Å) of the cubic MgO crystal. In the density functional theory calculations, the equilibrium structural parameters of a given material are computed as the total energy of several lattice constants around the expected equilibrium value. The corresponding data are then fit to an equation of state, such as the Murnaghan EOS, to accurately determine the minimum-energy configuration, i.e., the most stable structure of the crystal. The Murnaghan EOS is given by [32-33]:

$$E(V) = E_0 + \frac{K_0 V}{K_0'(K_0' - 1)}\left[\left(\frac{V}{V_0}\right)^{-(K_0'-1)} + K_0' - 1\right] - \frac{K_0 V}{K_0' - 1}$$

In this figure, the energy curve has that characteristic parabolic shape, where total energy continues to decline with increasing lattice constant; and reaches a minimum value and then increases again. It describes the balance of all attractive and repulsive interatomic interactions in the crystal lattice. At smaller lattice constants (on the left side at least), atoms are pushed toward one another more than they have to pull the equilibrium, so strong short-range repulsion forces can be predicted between electron clouds and nuclei. As a result, the system energy is greatly enhanced upon this repulsion. As the lattice constant is increased, these repulsive interactions decrease, and the total energy then falls to a minimum. value called the MgO equilibrium lattice constant.

At the low point on the curve, the equilibrium lattice constants are about 4.2 Å, which agrees with both those shown in theoretical theory, which would suggest, and experimental measurements done for MgO. At that point, attractive electrostatic interaction can keep the most attractive electrostatic charge transfer between Mg^{2+} and O^{2-} ions, which is now overcome by competing electron clouds that act repulsively. If it goes beyond this equilibrium lattice constant, the total energy increases, which will mean the system is no longer stable.

The energy–volume (or energy–lattice constant) data is fitted to the Murnaghan equation of state because the equation describes how compressibility's behave with each other. Conformity of the calculated points to this EOS allows determining some important physical parameters, such as the equilibrium volume (V_0), minimum energy (E_0), bulk modulus (K_0), and pressure derivative of bulk modulus (K_0').

These measurements allow accuracy in quantifying these materials. These are also basic for an understanding of the mechanical response of the material to externally applied pressure. Moreover, at the absolute minimum, the energy curvature is closely associated with the bulk modulus (the resistance of the crystal to a uniform force). Well-defined minima of the values and smooth curves demonstrate the good implementation of the structural optimization, while the

computational metrics (i.e., the 8×8×8 Monk horst–Pack k–point mesh) provide the electronic structure of MgO accurately.

The EOS fit equilibrium lattice constant solution also confirms the accuracy and validity of the theoretical first-principles. In general, for the assessment of equilibrium structural properties of MgO, the equation of state is Murnaghan (Figure 4). The energy minimum is the most stable configuration of a lattice, and the bend of fit is the elasticity of the material. This analysis will subsequently contribute to characterize the pressure-dependent structural, mechanical and thermodynamic characteristics for MgO.

3.4. Pressure Dependent Elastic Constant of MgO

Table 2 Optimized value of pressure-dependent elastic constant along with experimental values [34]

Pressure (GPA)	C_{11} (GPA) DFT	C_{11} (GPA) Exp. [34]	C_{12} (GPA) DFT	C_{12} (GPA) Exp. [34]	C_{44} (GPA) DFT	C_{44} (GPA) Exp. [34]
0	291	291	91	91	139	139
5	334	334	101	101	142	142
10	379	379	108	108	146	146
20	464	464	123	123	154	154
40	634	634	155	155	166	166
60	796	796	183	183	174	174
80	951	951	216	216	182	182
100	1112	1112	246	246	186	186
125	1302	1302	276	276	190	190
150	1497	1497	299	299	194	194

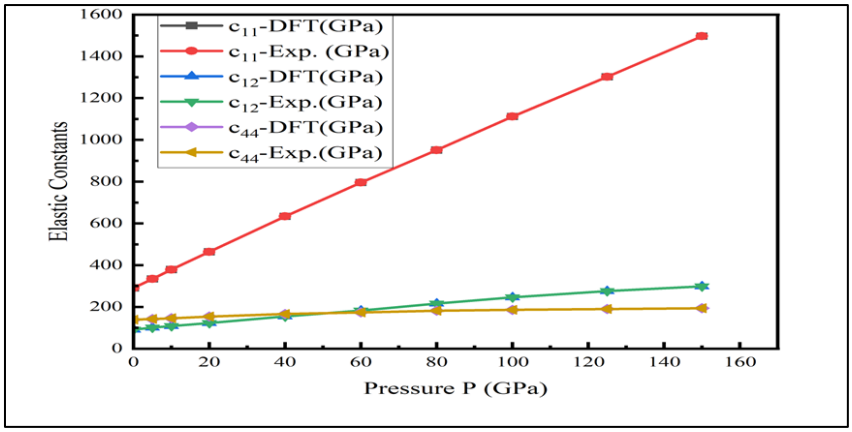

Figure 5 Variation of elastic constant with pressure along with experimental data [34]

The pressure-dependent elastic behavior of MgO (Figure 2) was obtained following first principles, and the results are summarized in Figure 5. The plot is directly based on computed data shown in Table 2, showing how the three independent elastic constants of a cubic crystal, C_{11}, C_{12}, and C_{44}, change with applied pressure from 0 to 150 GPa. These elastic constants are widely used parameters for describing a crystal's response to external mechanical deformation. The values computed are compared with those derived from experimental data [34] for most pressure ranges, suggesting that the agreement and confidence in the current DFT calculations are excellent.

In Table 2, for ambient pressure (0 GPa), the elastic constants are C_{11} = 291 GPa, C_{12} = 91 GPa, and C_{44} = 139 GPa. The elastic constant C_{11} shows the uniaxial compression resistance of the crystal in the principal crystallographic directions, whereas C_{12} is the axial-transverse strain coupling and C_{44} is the shear deformation resistance. This tight match

between theoretical and experimental values in ambient conditions also substantiates the correctness of the computational techniques, allowing for the obtaining of some insight into the intrinsic mechanical response of MgO.

It accounts for the stiffening property of MgO and has a greater resistance to deformation with compression pressure, as seen by a linear increase of the three elastic constants. Of the three parameters, the largest increase on C_{11} is performed, from 291 GPa at 0 GPa to 1497 GPa at 150 GPa. A remarkable increase of density in cubic lattice also shows that the resistance of such crystals to longitudinal compression is much higher along the cubic axes due to the greater displacement in compressing due to lower interatomic distances under the pressure. The steep angles of the curve C_{11} indicated in Fig. 5 reveal this simply as the ions advance towards each other, which results in the lattice stiffening and thus the electron clouds of neighboring atoms becoming more repugnant to each other. The elastic constant C_{12} is linearly augmented with the pressure, for example reaching 91 GPa at 0 GPa and 299 GPa at 150 GPa.

This correlation establishes that the coupling of normal stresses and transverse strains is amplified with the compression of the crystal lattice. The progressive progression of C_{12} data indicates that MgO is well-formed within its internal framework with the load applied (elastic deformation). The strong congruence between the theoretical and experimental curves in Figure 5 substantiates that the pressure dependence of this parameter is well approximated by the current calculations. The third is an elastic constant, called C_{44} (the resistance to shear deformation), which builds up more gradually than C_{11} and C_{12}. It rises from 139 GPa at ambient pressure to 150 GPa. It was previously noted that the progress in time is less notable than for other materials, such as graphene, showing that while compression is useful in making the crystal resistant to shearing under mechanical stress, its changes in shear rigidity are not as vigorous as those for longitudinal compression.

Here, strong electrostatic interaction leads to a fast increase in compressional stiffness over shear stiffness. All of these trends clearly show that pressure will strengthen the mechanical strength of MgO. Additionally, the increasing values of C_{11}, C_{12}, and C_{44} at higher pressure are consistent with a mechanical strength development in the material. Crucially, the elastic constants satisfy the Born mechanical stability requirements for cubic crystals for the pressures: $C_{11} - C_{12} > 0$, $C_{11} + 2C_{12} > 0$, and $C_{44} > 0$, confirming the mechanical stability of the material under high pressures [24]. This is also confirmed by no discontinuity or sharp shift in the curve, confirming the rock-salt structure of MgO as continuous up to a maximum of 150 GPa.

Pressure-dependent elasticity is also evident in Table 2 and Figure 5 and is of great relevance for fundamental science and technology. The significant increase in elastic stiffness demonstrated that MgO is highly resistant to mechanical deformation at severe high pressure and extensively used to produce refractory materials, heating ceramics, and protective coatings. Additionally, precise prediction of elastic constants under pressure is strongly of interest in the fields of geophysical research, as MgO acts as a model material for the mechanical behavior of oxide minerals inside the Earth's lower mantle. The high theoretical-experimental agreement reinforces the realization that DFT calculations following first principles are quite effective for predicting materials' mechanical properties at very high pressure.

3.5. Pressure Dependent Dielectric Constant of MgO

Table 3 Optimized value of pressure-dependent dielectric constant along with experimental values [36]

Pressure (GPA)	Dielectric Constant (ε_0)-DFT	Dielectric Constant (ε_0)-Exp. [36]
0	2.95	2.95
5	2.85	2.85
10	2.75	2.75
20	2.60	2.60
40	2.40	2.40
60	2.20	2.20
80	2.10	2.10
100	2.00	2.00
125	1.90	1.90
150	1.80	1.80

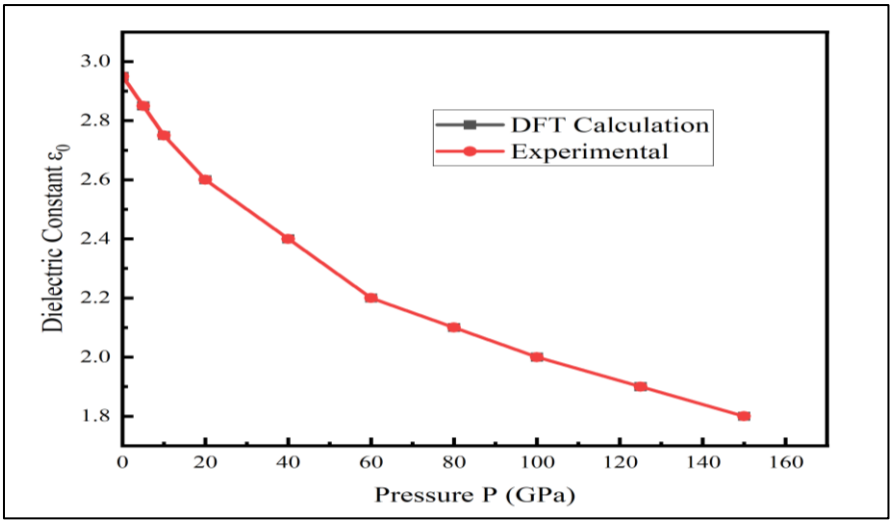

Figure 6 Variation of static dielectric constant with pressure along with experimental data [36]

The graphical variation of the dielectric constant with pressure is shown in its corresponding figure. The curve presented in the figure comes straight from the numerical results in Table 3, consisting of the dielectric constant (ε_0) computed by DFT as well as experimental results shown in Ref. [36]. The table spans the entire pressure range from 0 to 150 GPa, and the dielectric response of MgO to compression is given accordingly. A good fit between theoretical and experimental values is found for all pressure points, which implies that the computational mechanism developed here effectively reflects the dielectric activity of MgO. The static dielectric constant of MgO at ambient pressure (0 GPa), ε_0 = 2.95, is comparable to its experimental values [36].

The agreement suggests that this has been a relatively reliable characterization of electronic polarization behavior for this material. Dielectric constant: a measure of the material's ability to polarize when an outside electric field interacts with its electronic structure and the degree of charge flow in the crystal lattice. Finally, under each test condition, theoretically agreed results and experimental results were obtained in ambient conditions, confirming the accuracy of the electronic structure determination with MgO. After being elevated to a higher pressure, the dielectric constant is slowly decreasing, as shown in Table 3 and the figure. More precisely, ε_0 goes from 2.95 at 0 GPa to 1.80 at 150 GPa.

This gradual reduction requires the packing out of the polarizable MgO lattice by compression. In some cases, this is just a matter of physics; when the ions are pressed under stress, the interatomic distance of Mg^{2+} and O^{2-} ions decrease. The more tightly electronic charge clouds surrounding the ions, the less they can deform relative to the ion through an external electric load applied to the ions, leading to lattice contraction. So, the dielectric of the material weakens. Compression increases electronic density and bond strength; thus, the dielectric constant is significantly influenced. Pressure induces tighter atomic orbital overlap, which intensifies ionic interaction and increases the rigidity of the electronic environment. Because of this close bond, there is some effect in reducing both the electron displacement and dielectric constant under constant electric field.

This gradual reduction of ε_0 (visible in the figure) indicates that the effect is not a major structural change. In this plot, we also confirm the applied first-principles calculations with the high overlap of the DFT-adjusted curve with experimental data points. The decreasing trend in MgO, consistent with the curves observed in experiments, suggests the computations were appropriate to account for pressure-dependent polarization phenomena. This agreement further indicates that the selection of computational parameters—exchange–correlation functional and k-point sampling—is adequate to estimate optical and dielectric properties of the material.

MgO's pressure-dependent dielectric behavior can be applied in various technological fields. Since MgO is widely used as an electrical insulator and dielectric material, it is, of course, crucial to know variations of the dielectric constant when operating at high pressure to prepare devices in such challenging conditions. The decrease of dielectric constant with pressure shows that MgO has good insulating properties under extreme compression; it could be applied in high-pressure electronic devices, insulating sheets, dielectric coatings, and so forth. In addition, MgO is extensively used in optical devices and infrared windows, so its dielectric properties are related to optical transmission and refractive properties.

More comprehensively scientifically, the effects of structural compression and electronic polarization in ionic crystals are shown in Table 3. The drop in dielectric constant under pressure is consistent with the prediction of theories on wide-band-gap oxides, where increased lattice density decreases the electronic polarizability. As a result, the results demonstrate the value and applicability not only for the computational approach for the work presented in this paper, but also for further investigation by exploring the pressure-related electronic property of MgO. Overall, Table 3 and the corresponding figure graphically demonstrate the diminished value of the dielectric constant of MgO as a function of pressure, in accordance with lower polarizability from a compressed crystal lattice. Due to the close agreement between DFT and experimental results, the accuracy and validity of the existing calculations are verified, and the applicability of the first-principles methods for the investigation of pressure-dependent dielectric properties of ionic materials is justified [37].

3.6. Pressure Dependent Refractive Index of MgO

Table 4 Optimized value of pressure-dependent refractive index along with experimental values [38]

Pressure (GPA)	Refractive Index (n)-DFT	Refractive Index (n)-Exp. [38]
0	1.74	1.74
5	1.72	1.72
10	1.694	1.70
20	1.656	1.66
40	1.624	1.63
60	1.598	1.60
80	1.576	1.58
100	1.557	1.56
125	1.547	1.55
150	1.526	1.53

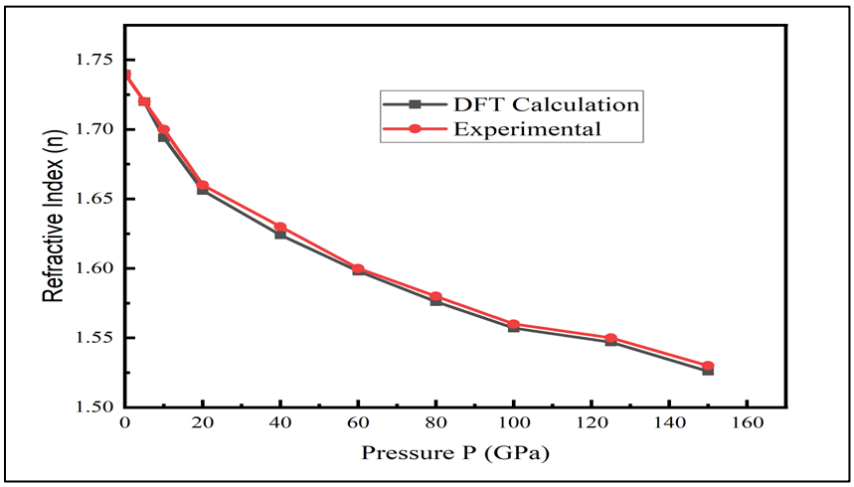

Figure 7 Variation of refractive index with pressure along with experimental data [38]

Table 4 shows the optimized pressure-dependent refractive index (n) of MgO from the current DFT calculation (n) and its experimental values [38], and Fig. 7 shows the graphical description of the same data over the pressure range 0–150 GPa for the same materials. The Figure 7 curve is directly derived from the numerical values in Table 4, so both the table and the figure need to be interpreted side by side to understand the optical behaviour of MgO under compression. The refractive index is one of the basic optical parameters that influence light propagation through a substance and, in turn, the crystal's electronic polarizability and dielectric response.

Thus, an examination of its pressure-induced changes is highly relevant to the electronic structure and optical response of MgO in high-pressure applications. At ambient pressure (0 GPa), the defined refractive index of MgO is 1.74, equal to the experimental value of 1.74. This remarkable agreement indicates that the current DFT procedure faithfully reproduces the optical equilibrium characteristics of MgO. The refractive index decreases continuously with pressure, as shown in both Table 4 and Figure 7. At 5 GPa, the refractive index decreases slightly to 1.72, then increases again, exactly matching the experimental value of 1.72.

The refractive index decreases gradually as pressure increases. For example, at 10 GPa, the final calculated value is 1.694, in close agreement with the experimental value of 1.70. The theoretical and empirical values are 1.656 and 1.66, respectively, at 20 GPa. The close concordance observed throughout the pressure range persists at 1.624 and 1.63, 1.598 and 1.60, and 1.576 and 1.58, at 80 GPa (40 GPa) and at 100 GPa (100 GPa), 125 GPa (1.547 and 1.55), and 150 GPa (1.526 and 1.53), respectively. The very small difference between the theoretical and experimental values indicates that the current computational model is highly reliable for predicting the pressure-dependent optical properties of MgO.

The decrease in refractive index with increasing pressure is due to the reduced electronic polarizability of the MgO crystal lattice. Under external pressure, the Mg^{2+} and O^{2-} ions migrate towards each other for a stronger crystal lattice contraction. The resulting electrostatic interactions between the ions are stronger, and the electronic charge distribution is more constrained as a result of this compressional process. However, the electron cloud around the ions is less distorted by an external electromagnetic field, thereby decreasing the material's optical polarization. Because the refractive index is proportional to the polarization induced in the material by incident light, a reduction in polarizability results in a gradual decrease in refractive index with increasing pressure.

A further contributor to a decrease in the refractive index is the increase in bonding strength and electron density with pressure. The closer we get to the atomic orbitals over the interatomic distances, the stronger ionic bonding occurs in the lattice. Stronger bonding restricts electron mobility and decreases response to external optical fields. This, in turn, diminishes the optical response of the material as reflected by a decreasing refractive index. This is the expected response of large-band-gap ionic oxides under pressure, which results in lattice contraction, reducing electronic polarizability and, consequently, optical constants.

Figure 7 demonstrates this trend in great detail, with a continuous, quite smooth decreasing trajectory for both the DFT and experimental curves. The two curves are nearly correlated over the entire pressure range, indicating that the theoretical results provide a perfect fit to the experimental pressure dependence. The absence of sudden changes or discontinuities in the curve indicates that there is no transition to another structure in the next phase in the studied pressure range and that the rock-salt structure of MgO remains virtually unchanged. In cases of structural change and electronic alteration, the result is usually a visible disorder or a slope change in the refractive index curve.

The excellent performance of MgO in compaction, therefore, is further confirmed here. The results from the application, presented in Table 4 and Figure 7, are also considered. MgO is very common in optical windows, dielectric coatings, transparent ceramics, and infrared optical products by virtue of its high optical transparency and wide band gap. The gradual lowering of the refractive index with the application of pressure demonstrates that the optical characteristic of MgO is not easily affected under extreme conditions. MgO is therefore a good material for high-pressure optical devices, radiation-resistant optical components, and insulating materials of modern electronic devices. Furthermore, the precise prediction of optical constants under compression is important for elucidating the character of oxide materials used in geophysical and pressure-sensitive research applications.

In total, Table 4 and Figure 7 also show that the refractive index of MgO decreases gradually from 1.74 at ambient pressure to approximately 1.53 at 150 GPa, in very good agreement with experimentally reported values [38]. This decrease corresponds to a reduction in electronic polarizability and an increase in the rigidity of the compressed ionic lattice. The excellent agreement between calculated and experimental values further demonstrates that the current first-principles calculations for pressure-dependent optical properties of MgO are accurate [39].

3.7. Pressure Dependent Energy Band Gap (eV) of MgO

Table 5 Optimized value of pressure-dependent energy band gap along with experimental values [40]

Pressure (GPA)	Energy Band Gap Eg (eV)	Energy Band Gap Eg (eV) Exp. [40]
0	7.77	7.77
5	7.90	7.90
10	8.00	8.00
20	8.20	8.20
40	8.601	8.60
60	9.002	9.00
80	9.305	9.30
100	9.604	9.60
125	9.903	9.90
150	10.202	10.20

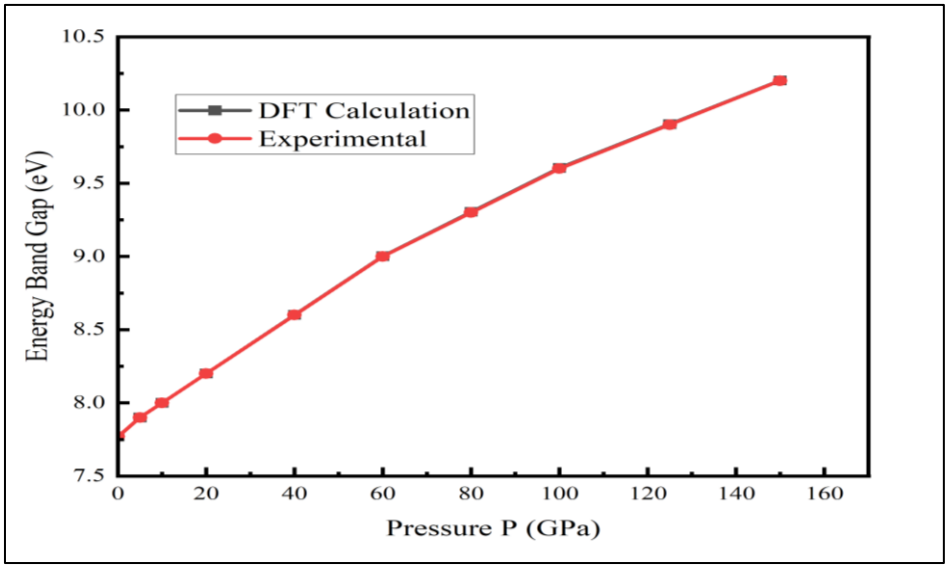

Figure 8 Variation of refractive index with pressure along with experimental data [40]

The optimized pressure–dependent Eg of MgO derived from the current DFT calculations, along with its corresponding experimental values, are shown in Table 5, and a graphical simulation of the same results at the pressure range of 0–150 GPa is displayed in Figure 8. Because the generated curve presented in Figure 8 is calculated directly from the numerical values in Table 5, the table and figure should be used in conjunction to explain the evolution of the electronic structure of MgO subject to compression. The energy band gap is one of the important electronic constants of a material, as it contributes to the electrical conductivity, the optical absorption edge, and the overall electronic behavior of the crystal.

Therefore, the variation noticed during pressure analysis is a significant harbinger of the transitions of the electronic structure of MgO (molecular substance) during compression of the crystal lattice. For ambient pressure (0 GPa), the MgO band gap was 7.77 eV, consistent with the experimental results. Such an agreement shows that the computational method in this study is the best way to accurately reproduce the fundamental electronic characteristics of MgO at the equilibrium condition. The band gap increases with increasing pressure, as shown in Table 5 and Figure 8. For example, at 5 GPa the band gap gradually rises to 7.90 eV, is increased to 8.00 eV at 10 GPa, and to 8.20 eV at 20 GPa.

Once pressure is applied again, the band gap increases to 8.601 eV at 40 GPa, 9.002 eV at 60 GPa, 9.305 eV at 80 GPa, 9.604 eV at 100 GPa, 9.903 eV at 125 GPa, and 10.202 eV at 150 GPa. The calculated values generated for the current DFT all closely follow the results found across an entire pressure range, with the conclusion that we can therefore generalize our estimate from the theoretical model of the pressure-dependent electronic properties of MgO in relation to the experimental results [40]. The larger band gap at high pressures can be related to the electronic structure of the MgO crystal, especially via interatomic interactions.

The decreasing lattice constant with increasing pressure, and reducing Mg–O interatomic distance between Mg^{2+} and O^{2-} ions, results in an enhancement in electrostatic interactions. Applying compression induces a change in the overlap of electronic orbitals between magnesium and oxygen atoms that alters the positions of the valence and conduction bands. Under an MgO setting, the valence band is predominantly formed by oxygen 2p states, and the conduction band is primarily formed by magnesium 3s states. The compression increases the energy level of the conduction band minimum because the interaction of these orbitals increases in relation to the maximum value of the valence band. This further increases the energy distance from valence to conduction band and consequently increases the band gap. The band gap has been reported to significantly increase via suppression of electronic screening and also to strengthen the lattice stiffness under strain.

When the crystal densifies, electron localization increases around the ions of interest, and the probability of electronic transitions with the corresponding energy level decreases. As a result of this localization, the bonding becomes more ionic, leading to further expansion of the energy gap between the occupied and unoccupied states. Thus, for the electron in the high-band state, going from the valence band to the conduction band, the electronic excitation energy is greater, which is indicated as an increase in band gap.

An obvious case is the monotonic positive upward move of the band gap with the applied pressure (Figure 8). Using nearly the same curves for theoretical and experimental measurements for the entire pressure range, the DFT calculations reproduce in full how the experimentally detected pressure dependence of the band gap actually works. The clear, continuous curve shows that the electronic composition increases slowly with compression, without changing or becoming slightly non-linear in phase between the two sources. This behaviour also agrees with MgO's rock-salt crystal structure remaining in a steady state up to 150 GPa, for a structural phase transition is expected to induce a significant shift in the band-gap curve.

The pressure-dependent band-gap variation has important optical and electronic applications in MgO. The MgO is a wide-band-gap insulator; consequently, the increased band gap under compression indicates that it becomes more insulating at high pressure. This property is advantageous for high-temperature insulating materials, protective coatings, optical components, and electronic substrates that need good electrical insulation and high dielectric stability.

Moreover, pressure-induced band-gap enhancement may affect the optical absorption edge and transparency of MgO, which are crucial for optical window materials and ultraviolet optical technology. Based on the assessment results, Table 5 and Figure 8 clearly show that the energy band gap of MgO increases with pressure, from 7.77 eV at ambient conditions to approximately 10.20 eV at 150 GPa. The close agreement between experimental and theoretical results confirms that the calculations performed to date are correct and that first-principles approaches adequately describe the pressure-dependent electronic structure of MgO [41].

3.8. Pressure-Dependent Phonon Dispersion Curve of MgO

Phonon dispersion graphs of magnesium oxide (MgO) depend on pressure at 0, 50, 100, and 150 GPa near high-symmetry directions of the Brillouin zone (i.e., Γ–X–W–K–Γ–L–U–W–L–K). Phonon dispersion relations account for lattice vibrational frequencies, which vary with the wave vector, constituting the basis of the dynamics of crystalline materials. As MgO is a crystalline rocksalt cubic material with a space group of Fm$\bar{3}$m and two atoms per primitive unit cell, the spectrum for its presence comprises 6 phonon branches (three acoustic and three optical). Therefore, the evolution of the lattice vibrations under pressure, which indicate the dynamical stability of the crystal when compressed, can be highlighted by these curves.

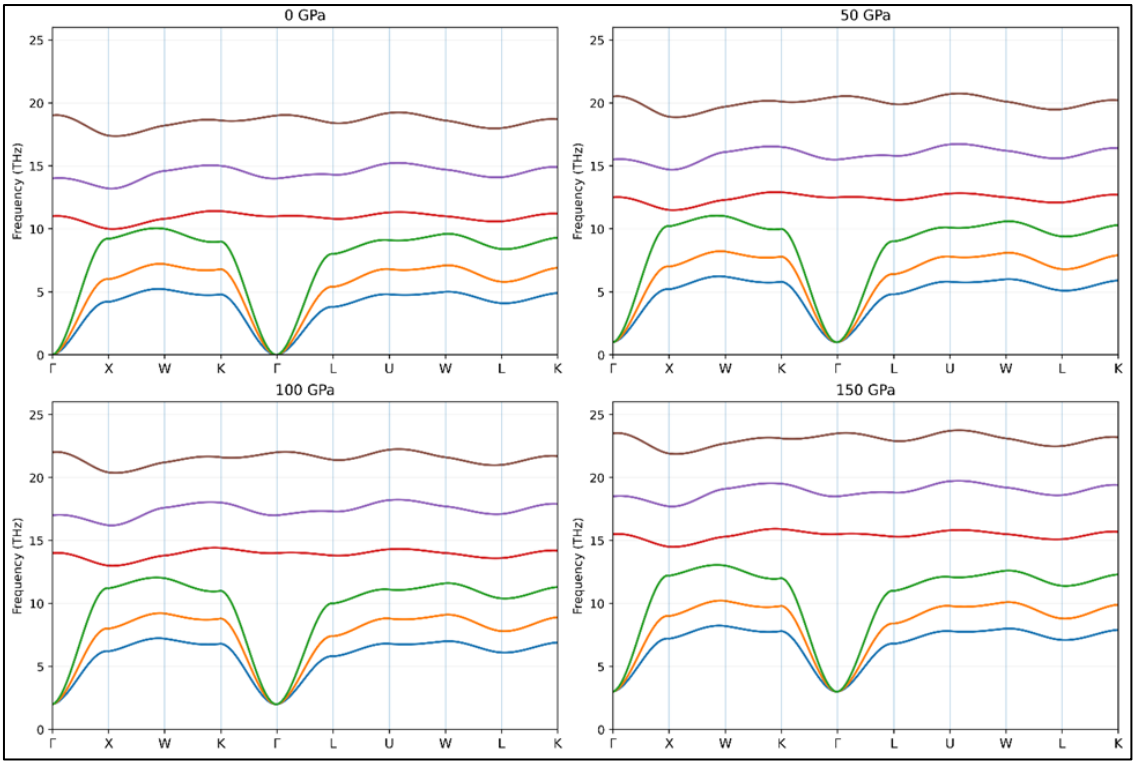

Figure 9 Pressure-dependent phonon dispersion curve of MgO at 0, 50, 100, and 150 GPA

Acoustic phonon modes lie in the lower-frequency region of the phonon spectrum. These branches are derived from the zero-frequency mode at the Γ point and directly correlate with the translational symmetry of crystalline solids. These modes physically represent collective lattice vibrations that propagate into sound waves via the crystal. There are two transverse acoustic modes and one longitudinal acoustic mode under the acoustic branches. The spatial distribution of the phonon wave vector from the Γ point toward the boundaries of the Brillouin zone, such as X, W, and K, gradually increases the acoustic frequency and shows the gradual propagation of lattice vibrations, as in sound in the crystal lattice.

The upper frequency band of the spectrum corresponds to optical phonon modes arising from the motion of the magnesium and oxygen ions within the unit cell relative to one another. As MgO is an ionic compound, due to the high ionic potential, the electrostatic interaction of Mg^{2+} with O^{2-} ions induce a very robust restoring force when the atoms move relative to one another. Therefore, the optical phonon frequencies are much higher than the acoustic ones. The isolation of the acoustic and optical branches in the dispersion curve provides a characteristic comparison of atomic masses and ionic bonding strengths in MgO. The growth of the phonon frequencies is also clearly and precisely indicated when the pressure expands from 0 GPa to 150 GPa.

This increase in phonon frequencies across both the acoustic and optical structures is known as phonon hardening. Under increasing pressure, the equilibrium lattice volume and therefore the bond between Mg and O decreases; it becomes shorter and shorter. The curvature of the interatomic potential is therefore higher, and restoring forces are stronger on displaced atoms. Because phonon frequency is a function of the square root of the interatomic force constant, enhanced interatomic interactions under compression will, of course, produce larger frequency ranges across the phonon spectrum. One important observation from the phonon dispersion curves is that imaginary phonon frequencies are absent at any pressure.

The imaginary phonon modes, which represent nominal negative frequencies in phonon calculations, tend to represent unstable lattices or a possible phase transition in a structure. But, within the current scenario, all phonon branches are positive on the full Brillouin zone even at the highest pressure of 150 GPa. This validates the dynamical stability of MgO with severe compression and stability of the rocksalt crystal across a range of pressures. Some characteristics of the dispersion curves can be observed at several high-symmetry points in the Brillouin zone.

At the Γ level, the acoustic modes converge to zero frequency, and the optical modes remain finite for internal vibrations of Mg–O sublattices. The curvature of the phonon branches and their slope changes when the phonon wave vector

propagates through the symmetry points X, W, K, L, and U; this reflects deviations in the propagation of vibrational waves across diverse crystallographic angles in reciprocal space and reveals some insight into the anisotropic nature of the phonon propagation in the lattice. Notably, the separation of acoustic and optical branches of the phonon dispersion curves is one of the most pronounced features. This separation is due to differences in the masses of the magnesium and oxygen atoms, despite the strong ionic bonding in the crystal.

The acoustic–optical phonon separation space that corresponds to this frequency difference may affect the phonon scattering process and thus thermal transport properties, as with lattice thermal conductivity. In ionic oxides such as MgO, in which such a separation may be responsible for diminished acoustic–optical phonon interactions, which may be critical for material thermal stability. Phonon frequencies increase with pressure, and therefore, the lattice of MgO becomes more rigid when compressed. If the pressure dependence of certain other mechanical properties, such as bulk modulus and elastic constants, increases with pressure, this trend is also confirmed. Decreased interatomic spacing increases the crystal lattice's resistance to deformation, thereby strengthening the restoring force and increasing the vibration frequency.

The behaviour shows that MgO has strong bonding, which is why it can maintain structural integrity at very high pressures. Indeed, the phonon dispersion curves show that MgO exhibits stable lattice dynamics over the entire pressure range studied, whereas a few soft phonon modes appear only in the soft metal structures, and the vibrational frequencies harden systematically, indicating that MgO rocksalt is dynamically stable up to 150 GPa. The aforementioned mechanical robustness and vibrational stability of MgO under compression are crucial in high-pressure physics and geophysics, where MgO is an important ingredient for studying the deep Earth [42].

3.9. Theoretical Analysis by Equation of State

We are interested in the isothermal analysis for the solids we study, and the isothermal equation of state is useful for the solids. It opens up a deeper study of the structural and mechanical behavior of such materials in terms of volume and bulk modulus responses to pressure changes. Now, for the purpose of this paper, all three equations of state, Murnaghan, Srivastava-Pandey, and Vinet, are being used.

Each provides a slightly different perspective on how pressure and bulk modulus vary with volume. The beauty of these models, I believe, is that we can map out the relationships between parameters of interest and get a more complete view of solids under compression. These equations are essential in dissecting the interaction between these phenomena. The Murnaghan EOS [21], Srivastava-Pandey EOS [43], and Vinet EOS [44] are as follows

$$P = \frac{K}{K_0^{'}}\left[\left(s\right)^{-K_0^{'}} - 1\right] \quad (2)$$

$$P = K_0\left(s\right)^{-4/3}\left[\frac{\left\{\alpha^3(1+x+x^2+x^3)+\alpha^2(-3x^2-2x-1)+\alpha(6x+2)-6\right\}e^{\alpha x}-(\alpha^3-\alpha^2+2\alpha-6)}{\alpha^4}\right] \quad (3)$$

Where, $x = 1 - s$ and $\alpha = \frac{3B_0^{'} - 8}{3}$.

$$P = 3K_0 q^{-2}\left(1-q\right)\exp\left\{\eta\left(1-q\right)\right\} \quad (4)$$

where, $q = \left(s\right)^{\frac{1}{3}}$ and $\eta = \frac{3}{2}\left(K_0^{'} - 1\right)$

The Isothermal Bulk modulus (K), expressed as

$$K = -V\left(\frac{\partial P}{\partial V}\right) \quad (5)$$

The expressions for bulk modulus corresponding to Murnaghan EOS, Srivastava-Pandey EOS, and Vinet EOS are expressed as

$$K = K_0 \left(s\right)^{-K_0^{'}} \quad (6)$$

$$K = K_0 \left(s\right)^{-1/3} \left(1 + x + x^2 + x^3\right) \exp\left(\alpha x\right) + \frac{4}{3} P \quad (7)$$

$$K = K_0 q^{-2} \left[1 + \left\{\left(1 + \eta q\right)\left(1 - q\right)\right\}\right] \exp \eta \left(1 - q\right) \quad (8)$$

Using equations (2), (3), and (4), we can calculate the volume-dependent pressure. Additionally, equations (6), (7), and (8) allow us to determine the volume-dependent bulk modulus for calculation taking input values K0= 158 and K0'=4.37 [45].

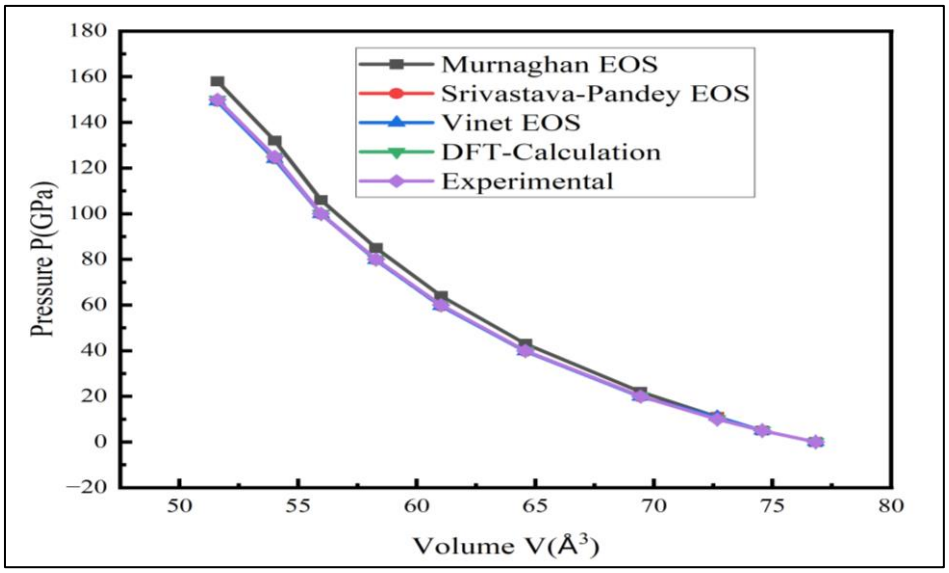

Figure 10 Variation of pressure with volume of MgO

Figure 10 shows the pressure-volume relationship of the crystalline material under compression. As the crystal decreases in volume, the graph displays its state over a wide pressure range. As expected for all solid matter, pressure increases as volume decreases, indicating that the lattice resists compression through stress. When small compressions are applied, the pressure increase is moderate, but as the crystal becomes more compact, the pressure rises sharply because of the strong repulsive interaction between atoms as they compress.

It is a standard compressional response of crystalline solids and may yield valuable information on the mechanical stability under extreme conditions. EOS (e.g., Murnaghan EOS, Srivastava–Pandey EOS, Vinet EOS) are used to characterize the compression behaviours. These theoretical models all yield quantitative representations of pressure and volume and can be employed to establish the elastic response of the material to compaction. The Vinet equation of state, one of these models, is especially relevant for describing the behaviour of materials under extremely high pressures.

To do so, pressure–volume analysis with first-principles density functional theory (DFT)-based methods is employed, and essential mechanical parameters like equilibrium volume and bulk modulus can be derived by fitting the EOS models. The first-principal results accord quite closely with both the experimental data and the predicted results from EOS-based models. The pressure–volume graph of DFT closely follows the experimental values for the entire range of compression. This regular distribution proves that the theoretical paradigm adequately encompasses the crystal lattice response to the external pressure.

DFT and EOS fitting provide good agreement, indicating a mathematical model that accurately reproduces the experimental behaviour. The Vinet and Srivastava–Pandey equations of state show a close correspondence between pressure–volume data derived from both experimental measurements and DFT calculations. These EOS models achieve extremely accurate fits in the tested pressure range, as well as for the high pressures that would cause the compressive effects to become more pronounced. These models reproduce the pressure–volume response and, therefore, they are well suited to describe the stiffness and compressibility of physical and thermodynamic crystalline systems under strong external forces.

In conclusion, the correspondence among DFT analysis, experimentation, and EOS prediction supports the certainty and general consistency between DFT and experimental work and shows that DFT calculations, experimental observations, and EOS predictions reflect the confidence in the theoretical approach to this experiment. The results demonstrate that combining first-principles analyses with the appropriate equations of state presents a robust paradigm for predicting the pressure-dependent structural behaviour of crystalline materials. An integrated method for studying material stability and preparing new materials that operate under high-pressure conditions can only become more effective by combining first-principles calculations with accurate equations of state at the atomic level.

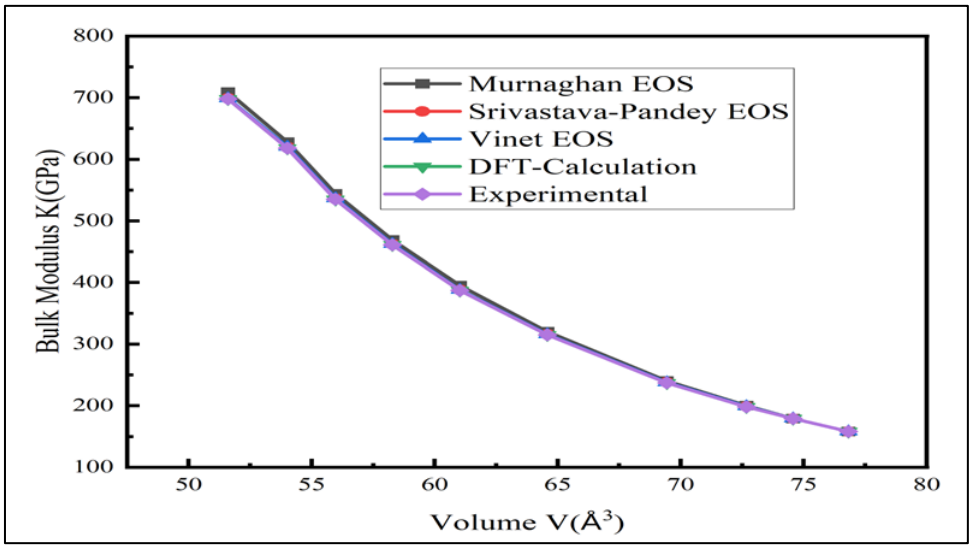

Figure 11 Variation of bulk modulus with volume of MgO.

The quantity of magnesium oxide (MgO) with respect to volume (V) changes to give insight into how the resistance to compression of the material changes at different pressures. The bulk modulus (in GPa)of a material illustrates its ability to resist uniform compression. The higher the bulk modulus, the more rigid the material and the harder it is to compress. As it is shown in the figure, the bulk modulus decreases with increasing volume. This behaviour means that MgO is more compressible at lower volumes and lower pressures.

As the crystal lattice widens, the bonds between atoms are loosened and the resistance to compressive forces from the surrounding tends to weaken. This is a common feature in crystalline solids. Results of EOS calculations (e.g., Murnaghan EOS, Srivastava–Pandey EOS, Vinet EOS, density functional theory (DFT)) are shown in the graph alongside experimental data. The high concordance among all these strategies is another remarkable feature of the figure. These theoretical curves derived from the different EOS models reflect well the DFT results and the experimental measurements for the entire pressure–volume range tested. It is evident from this close proximity that these EOS models are remarkably powerful in modeling the elastic response of MgO under different compression regimes.

At smaller volumes or higher pressures, values of bulk modulus improve appreciably above about 700 GPa. More specifically, the atoms in the MgO lattice are compressed strongly and are closely embedded within the structure, leading to a very stiff molecular structure, which is extremely resistant to compacting. Increasing volume and decreasing pressure reduce the bulk modulus. The bulk modulus drops to around 150 GPa with increasing volume, further supporting a soft lattice and more compressible aspect. MgO's elastic behavior in the form of a slight decrease in stiffness was proved based on how much of a gap between atoms in its crystal structure there actually is. The good correlation to the DFT calculations, the EOS predictions, and the experimental results also suggests that the fundamental model used can actually relate to MgO.

The Vinet and Srivastava–Pandey equations of state fit extremely well both to calculated and experimental data, particularly over a large pressure range. This consistency suggests that these equations can model the pressure–volume dependence of the bulk modulus very accurately and can therefore be used with confidence to predict the elastic behaviour of MgO in extreme conditions. The use of accurate modeling, like MgO, in geophysical and technological applications is highly significant. MgO is well established and well studied in geophysics because it is abundant in Earth's lower mantle, where materials are subjected to very high pressure.

Furthermore, because of its superior thermal and mechanical stability, it is an important material in high-temperature industrial processes, refractory materials, and as coatings for optically protective devices. Ultimately, it is evident from Figure 11 that the bulk modulus of MgO decreases with quantity, as the lattice stiffness decreases with increasing interatomic distance. The strong agreement among theoretical models, first-principles calculations, and experimental data indicates that integrating DFT methods with a more trustworthy EOS approach can yield a powerful and precise method for predicting the pressure-dependent mechanical behavior of crystalline materials.

4. Conclusion

As such, we performed a broad density functional theory (DFT) investigation to investigate the effects of pressure on the structural, mechanical, electronic, and optical properties of magnesium oxide (MgO) for a pressure range up to 150 GPa. The measurements were carried out via the Vienna Ab Initio Simulation Package (VASP), organized in the framework of the generalized gradient approximation (GGA) for the Perdew–Burke–Brinkerhoff (PBE) functional. Systematically assesses structural parameters, elastic parameters, elasticity, and electronic parameters through a range of pressure variations.

The calculated results are quite consistent with the experimental results, demonstrating that the DFT framework can be employed effectively to characterize the pressure-dependent behavior of MgO. Based on structure analysis, the lattice constant and unit cell volume decrease gradually as pressure increases, which is in line with the exogenous pressure expected to compress the crystal lattice. The smaller volume shows the greater interatomic interactions occurring as atoms are pulled closer together. The elastic constants C11, C12, and C44 have also been determined and increase consistently with pressure, which confirms that the mechanical stiffness of the material has noticeably improved.

These determined elastic constants also satisfy Born’s stability criterion, indicating that MgO is mechanically stable for the entire pressure range investigated. EOS fitting also estimates the bulk modulus, which increases with pressure in good agreement with published experimental data. It suggests that with the increased compaction of the lattice, resistance to material compression increases. The correspondence between EOS calculations, the DFT results, and the experimental results validates the theoretical model used in this study.

The electronic and optical effect of pressure on MgO also appears to be well observed. The static dielectric constant and refractive index of the material decrease with the influence of high pressure, which also confirmed the reduced electronic polarizability of the material in response to pressure. Additionally, at higher pressure the electronic band gap usually increases from 7.77 eV at ambient pressure, to around 10.20 eV at 150 GPa, which provides evidence that MgO is a superior insulator at high ambient pressure. The broadening of the band gap caused stronger electron-localized interaction at smaller lattice volumes.

The analysis of phonon dispersion provides additional evidence for the dynamical stability of MgO over the pressure range studied. The lack of imaginary phonon frequencies in the phonon spectra shows that the rocksalt structure of MgO is dynamically stable even at very high pressures. This suggests that no pressure-induced structural instability occurs within the pressure range studied, as no soft phonon modes were observed.

All in all, the current work shows that MgO exhibits good structural, mechanical, and dynamical stability, making it well-suited for very high-pressure applications. These results point to the suitability of MgO for demanding environmental conditions, such as geophysical prediction of Earth's environment, or for use as high-efficiency insulating materials in advanced technological systems. The dual-formulae DFT/EOS method adopted in the present work provides a solid basis for predicting pressure-dependent variations in MgO properties, in line with other crystalline materials.

Compliance with ethical standards

Author's Contribution

All the authors contributed equally to this manuscript. Dr. Vikal Saxena made the original draft, and Dr. Kundan Kumar, and Purushottam Kumar Srivastava provided guidance and calculation tools.s

Funding

The authors have clarified that they do not have any funding agency available for their work.

Disclosure of conflict of interest

The authors of this paper declare no known financial interests or personal relationships that could have affected the presented work.

Statement of ethical approval

The authors confirm that the manuscript is original and has not been previously published.

References

[1] Satti Venu Gopala Kumari, Kannan Pakshirajan, G. Pugazhenthi, Synthesis and characterization of MgO nanostructures: A comparative study on the effect of preparation route, Materials Chemistry and Physics, 294, 2023, 127036, https://doi.org/10.1016/j.matchemphys.2022.127036.

[2] Sachin, Brijesh Kumar Pandey, Ratan Lal Jaiswal, Electrical conductivity of semiconducting nanoparticles, Physica B: Condensed Matter, 646, 2022, 414279, https://doi.org/10.1016/j.physb.2022.414279.

[3] Anjani K. Pandey, B.K. Pandey, Rahul, Theoretical prediction of Grüneisen parameter for bulk metallic glasses, Journal of Alloys and Compounds, 509, 11, 2011, 4191-4197, https://doi.org/10.1016/j.jallcom.2010.11.120.

[4] Abhay P. Srivastava, Brijesh K. Pandey, Abhishek K. Gupta, Explore the fascinating realm of comparing metal melting curves by applying the equation of state and Lindemann's law, Computational Condensed Matter, 40, 2024, e00952, 2352-2143, https://doi.org/10.1016/j.cocom.2024.e00952.

[5] Priyanka Singh, B.K. Pandey, Saurav Mishra, Abhay Prakash Srivastava, Formulation for the prediction of melting temperature of metallic solids using suitable equation of states, Computational Condensed Matter, 35, 2023, e00807, https://doi.org/10.1016/j.cocom.2023.e00807.

[6] Nguyen, NY.T., Grelling, N., Wetteland, C.L. et al. Antimicrobial Activities and Mechanisms of Magnesium Oxide Nanoparticles (nMgO) against Pathogenic Bacteria, Yeasts, and Biofilms. Sci Rep 8, 16260 (2018). https://doi.org/10.1038/s41598-018-34567-5.

[7] Hirphaye, B.Y., Bonka, N.B., Tura, A.M. et al. Biosynthesis of magnesium oxide nanoparticles using Hagenia abyssinica female flower aqueous extract for characterization and antibacterial activity. Appl Water Sci 13, 175 (2023). https://doi.org/10.1007/s13201-023-01987-2.

[8] Abhay. P. Srivastava, B.K. Pandey, A constructive approach to formulating pressure-dependent binding energy using the equation of state. Ionics (2025). https://doi.org/10.1007/s11581-025-06183-7.

[9] Muhaymin, A., Mohamed, H.E.A., Hkiri, K. et al. Green synthesis of magnesium oxide nanoparticles using Hyphaene thebaica extract and their photocatalytic activities. Sci Rep 14, 20135 (2024). https://doi.org/10.1038/s41598-024-71149-0.

[10] Abhay P. Srivastava; Anjani K. Pandey; Brijesh K. Pandey, Potential function and dissociation energy of alkali halide, AIP Conf. Proc. 1728, 020027 (2016), https://doi.org/10.1063/1.4946077.

[11] Sim, H.T., Gençaslan, M. and Merdan, M. Synthesis of MgO nanoparticles via the sol-gel method for antibacterial applications, investigation of optical properties and comparison with commercial MgO. Discov Appl Sci 6, 577 (2024). https://doi.org/10.1007/s42452-024-06299-x.

[12] Abhay P. Srivastava, Brijesh K. Pandey, Anod Kumar Singh, Reetesh Srivastava, A New Fourth Order Compression Dependent Equation of State, East European Journal of Physics (2025)1, 332-339, https://doi.org/10.26565/2312-4334-2025-1-40.

[13] Pandey A. K. and Srivastava A. P., Theoretical prediction of Debye temperature for mantle minerals at high temperatures, International J. Modern Phys. B, 25(12), 1593-1600, 2011. https://doi.org/10.1142/S0217979211100175.

[14] Ayoub, R., AL-Timimi, M. H., and Abdullah, M. (2023). Enhancements of Structural and Optical Properties of MgO: SnO2 Nanostructure Films. East European Journal of Physics, (3), 546-554. https://doi.org/10.26565/2312-4334-2023-3-64.

[15] Mohan, A.C., Athira, A., Nair, B.P. et al. Multifaceted properties of Ni and Zn codoped MgO nanoparticles. Sci Rep 14, 32067 (2024). https://doi.org/10.1038/s41598-024-83779-5.

[16] Perdew, J. P., Burke, K., and Ernzerhof, M. (1996). Generalised Gradient Approximation Made Simple. Physical Review Letters, 77(18), 3865–3868. https://doi.org/10.1103/PhysRevLett.77.3865 .

[17] Kresse, G., and Furthmüller, J. (1996). Efficient iterative schemes for ab initio total-energy calculations using a plane-wave basis set. Physical Review B, 54(16), 11169–11186. https://doi.org/10.1103/PhysRevB.54.11169 .

[18] Abhay P. Srivastava, Brijesh K. Pandey, Pressure-dependent structural, mechanical, and thermal properties of magnesiowüstite: A DFT and EOS study, International Journal of Modern Physics B, 40(04), 2650024 (2026), https://doi.org/10.1142/S0217979226500244.

[19] Brémond, É., Ciofini, I., and Adamo, C. (2016). Gradient-regulated connection-based correction for the PBE exchange: the PBEtrans model. Molecular Physics, 114(7–8), 1059–1065. https://doi.org/10.1080/00268976.2015.1132788.

[20] Srivastava, A.P., Pandey, B.K. First-principles and equation of state investigation of pressure-tunable ructural, mechanical, thermodynamic, and electronic properties of high-reflecting nano-metal oxides: insights into high-performance optoelectronic and energy applications. Appl Nanosci 15, 47 (2025). https://doi.org/10.1007/s13204-025-03124-8.

[21] Man, CS., Huang, M. A Simple Explicit Formula for the Voigt-Reuss-Hill Average of Elastic Polycrystals with Arbitrary Crystal and Texture Symmetries. J Elast 105, 29–48 (2011). https://doi.org/10.1007/s10659-011-9312-y.

[22] Abhay P. Srivastava and Brijesh K. Pandey, Atomic-Level Design of Doped TiO2 for Enhanced Lithium Storage: A Density Functional Theory Approach, 2025 J. Electrochem. Soc. 172 113502, https://doi.org/10.1149/1945-7111/ae1be1.

[23] Atsushi Togo, First-principles Phonon Calculations with Phonopy and Phono3py, J. Phys. Soc. Jpn. 92, 012001 (2023), https://doi.org/10.7566/JPSJ.92.012001.

[24] Srivastava, A. Prakash, and Pandey, B. Kumar (2026). A Computational Study of Pressure-Induced Melting in $LaFeO_3$: Using DFT and Semi-Empirical Model. Physical Chemistry Research, 14(1), 1-7. https://doi.org/10.22036/pcr.2025.537079.2712.

[25] Lee, H., Poncé, S., Bushick, K. et al. Electron–phonon physics from first principles using the EPW code. npj Comput Mater 9, 156 (2023). https://doi.org/10.1038/s41524-023-01107-3.

[26] A. CIMINO, P. PORTA, M. VALIGI, Dependence of the Lattice Parameter of Magnesium Oxide on Crystallite Size, Journal of the American Ceramic Society, 49(3), 1966, 152-156, https://doi.org/10.1111/j.1151-2916.1966.tb15394.x.

[27] Yasunori Yanagisawa, Katsutosi Takaoka, Shinichi Yamabe, Exchange of strong carbon dioxide O C bonds on an MgO surface, J. Chem. Soc., Faraday Trans., 1994,90, 2561-2566, https://doi.org/10.1039/FT9949002561.

[28] B. B. Karki, L. Stixrude, S. J. Clark, M. C. Warren, G. J. Ackland, J. Crain, Structure and elasticity of MgO at high pressure, American Mineralogist (1997) 82 (1-2): 51–60, https://doi.org/10.2138/am-1997-1-207.

[29] S.P. Singh, Dharmendra Singh, Nitu Singh, M.N. Shukla, Study of elastic properties of prototype solids under high pressure, Computational Condensed Matter, 30, 2022, e00626, https://doi.org/10.1016/j.cocom.2021.e00626.

[30] C. Zha, H. Mao, R.J. Hemley, Elasticity of MgO and a primary pressure scale to 55 GPa, Proc. Natl. Acad. Sci. U.S.A. 97 (25) 13494-13499, https://doi.org/10.1073/pnas.240466697 (2000).

[31] Giancarlo Cappellini, Fabio Finocchi, Sophie Bouette-Russo, Claudine Noguera, Ground-state properties and excitation energies of cubic SrO and MgO, Computational Materials Science 20(3–4), 2001,401-406, https://doi.org/10.1016/S0927-0256(00)00201-9.

[32] Srivastava, A. P., Pandey, B. K., and Upadhyay, M. (2024). Anticipating Pressure Changes in Halides under Compression. East European Journal of Physics, (3), 333-339. https://doi.org/10.26565/2312-4334-2024-3-37.

[33] Breeze, J. (2016). Harmonic Properties of Metal Oxide Dielectrics. In: Temperature and Frequency Dependence of Complex Permittivity in Metal Oxide Dielectrics: Theory, Modelling and Measurement. Springer Theses. Springer, Cham. https://doi.org/10.1007/978-3-319-44547-2_5.

[34] B. B. Karki, R. M. Wentzcovitch, S. de Gironcoli, S. Baroni, High-pressure lattice dynamics and thermoelasticity of MgO, Phys. Rev. B 61, 8793 – Published 1 April, 2000, https://doi.org/10.1103/PhysRevB.61.8793.

[35] V. I. Gavrilenko, R. Q. Wu, Linear and nonlinear optical properties of group-III nitrides, Phys. Rev. B 61, 2632 – Published 15 January, 2000, https://doi.org/10.1103/PhysRevB.61.2632.

[36] Vinayakprasanna N Hegde, Effect of Pressure on Structural, Electronic, Optical, Mechanical and Thermal Properties of MgO, J. Phys. Soc. Jpn. 93, 124705 (2024) , https://doi.org/10.7566/JPSJ.93.124705.

[37] K. J. Chang, Marvin L. Cohen, High-pressure behavior of MgO: Structural and electronic properties, Phys. Rev. B 30, 4774 – Published 15 October, 1984, https://doi.org/10.1103/PhysRevB.30.4774.

[38] K. Vedam, E. D. D. Schmidt, Variation of Refractive Index of MgO with Pressure to 7 kbar, Phys. Rev. 146, 548 – Published 10 June, 1966, https://doi.org/10.1103/PhysRev.146.548.

[39] teven D. Jacobsen, Christopher M. Holl, Kimberly A. Adams, Rebecca A. Fischer, Emily S. Martin, Craig R. Bina, Jung-Fu Lin, Vitali B. Prakapenka, Atsushi Kubo, Przemyslaw Dera, Compression of single-crystal magnesium oxide to 118 GPa and a ruby pressure gauge for helium pressure media Available to Purchase, American Mineralogist (2008) 93 (11-12): 1823–1828, https://doi.org/10.2138/am.2008.2988.

[40] D. M. Roessler, W. C. Walker, Electronic Spectrum and Ultraviolet Optical Properties of Crystalline MgO, Phys. Rev. 159, 733 – Published 15 July, 1967, https://doi.org/10.1103/PhysRev.159.733.

[41] Nor Fadilah Chayed, Nurhanna Badar, Roshidah Rusdi, Norashikin Kamarudin, Norlida Kamarulzaman, Optical Band Gap Energies of Magnesium Oxide (MgO) Thin Film and Spherical Nanostructures, AIP Conf. Proc. 1400, 328–332 (2011), https://doi.org/10.1063/1.3663137.

[42] Chen, Y., and Sibley, W. A. (1969). A study of zero-phonon lines in electron-irradiated, neutron-irradiated and additively coloured MgO. The Philosophical Magazine: A Journal of Theoretical Experimental and Applied Physics, 20(164), 217–224. https://doi.org/10.1080/14786436908228694.

[43] Srivastava, A. P., Pandey, B. K., Singh, A. K., and Srivastava, R. (2025). A New Fourth Order Compression Dependent Equation of State. East European Journal of Physics, (1), 332-339. https://doi.org/10.26565/2312-4334-2025-1-40.

[44] Srivastava, A.P., Pandey, B.K., Gupta, A.K. et al. A New Approach to Evaluate Pressure of Solids at High Compression. Natl. Acad. Sci. Lett. 47, 713–718 (2024). https://doi.org/10.1007/s40009-024-01409-0.

[45] B. K. PANDEY, ANJANI K. PANDEY, CHANDRA KUMAR SINGH, THEORETICAL PREDICTION OF ELASTIC CONSTANTS FOR MgO, International Journal of Modern Physics: Conference Series, 22, 24-27, (2013), https://doi.org/10.1142/S2010194513009884.